ChemistrySelect

Research Article
doi.org/10.1002/slct.202303328

Chemistry Europe
European Chemical Societies Publishing

www.chemistryselect.org

Investigation of Antimicrobial Activity and Cytotoxicity of Silver Nanoparticle Synthesized using Dopamine as a Reducing and Capping Agent

Ndivhuwo P. Shumbula,*[a, b] Zakhele B. Ndala,[b] Siyabonga S. Nkabinde,[c] Obakeng Nchoe,[b] Siyasanga Mpelane,[d] Poslet M. Shumbula,[e] Sindisiwe F. Muthwa,[f] Phumlani S. Mdluli,[a, f] Pumza Mente,[g] Zikhona Njengele-Tetyana,[a] Phumlani Tetyana,[a] Mbuso Mlambo,*[a] and Nosipho Moloto[b]

We present a study focused on the controlled fabrication of silver nanoparticles (AgNPs) through colloidal synthesis, employing dopamine as a reducing and capping agent. By manipulating the concentration of silver nitrate, the production of spherical AgNPs with distinct particle diameters (16, 24, 48, and 74 nm) was achieved. The investigation extended to the evaluation of AgNPs' impact on human embryonic kidney cells, revealing a concentration-dependent response. At lower AgNPs concentrations, cell viability remained nearly 100%, progressively declining with rising AgNPs concentrations. Importantly, the cytotoxic thresholds observed were notably elevated, underscoring the relatively mild to moderate toxicity profile of the nanoparticles. Furthermore, the antimicrobial efficacy of these synthesized AgNPs was probed against *E. coli* and *S. aureus* bacterial strains. Notably, the AgNPs exhibited robust antimicrobial activity, with superior performance exhibited by smaller-sized particles compared to larger ones. Impressively, the minimum inhibitory concentration reached as low as 3.5 μg/mL, indicating their potent antimicrobial potential. The achieved distinct particle diameters, concentration-dependent cytotoxic responses, and potent antimicrobial efficacy against bacterial strains underscore the multifaceted potential of these nanoparticles. These findings contribute valuable insights for their application in diverse fields, from biomedicine to antimicrobial solutions.

1. Introduction

The outbreak of infectious diseases caused by pathogenic bacteria and the development of new antibiotic-resistant strains have posed a risk to human health. New and effective antimicrobial materials need to be developed to tackle the health hazards caused by pathogenic bacteria.[1–4] The past few decades have witnessed a plethora of various synthetic antimicrobial active materials, thanks to nanoscience and nanotechnology[3,5,6]. Synthesis of nano-based materials introduces characteristics and properties that cannot be imagined in bulk materials. Silver (Ag), in the form of silver sulphadiazine, silver nitrate, or silver-polymer composites, has been widely studied and believed to be the most effective metallic antimicrobial agent.[7–9] In its nanoscale, Ag has caught scientists' and researchers' attention in various fields, including biochemistry, biology, and microbiology as antimicrobial agents.[1,6,10,11]

The antimicrobial activity of AgNPs has been widely investigated in the past years. AgNPs possess a broad inhibitory spectrum against microorganisms such as viruses, fungi, and bacteria. AgNPs as an antimicrobial agent can be a potential solution to improve antibiotic activity since most pathogens develop resistance with time.[1] For instance, *Salmonella typhi* (*S. typhi*) has developed resistance against chloramphenicol, ampicillin, quinolone, and trimethoprim.[12] Methicillin and fluconazole have lost their activity towards *Staphylococcus aureus (S. aureus)* and *Candida albicans* (*C. albicans*).[13] More-

[a] *N. P. Shumbula, P. S. Mdluli, Z. Njengele-Tetyana, P. Tetyana, M. Mlambo*
Health Platform, Advanced Materials Division, Mintek, 200 Malibongwe Drive, Randburg 2194, South Africa
Tel: +2711 709 3040
E-mail: ndivhuwos@mintek.co.za
mbusom@mintek.co.za

[b] *N. P. Shumbula, Z. B. Ndala, O. Nchoe, N. Moloto*
Molecular Sciences Institute, School of Chemistry, University of the Witwatersrand, Private Bag 3, Wits, 2050, South Africa

[c] *S. S. Nkabinde*
Hydrometallurgy Division, Mintek, 200 Malibongwe Drive, Randburg 2194, South Africa

[d] *S. Mpelane*
Analytical Facility, University of Johannesburg, P.O. Box: 524, Auckland Park 2006, South Africa

[e] *P. M. Shumbula*
Department of Chemistry, University of Limpopo, Private Bag x1106, Sovenga 0727, South Africa

[f] *S. F. Muthwa, P. S. Mdluli*
Faculty of Applied Sciences, Durban University of Technology, P O Box 1334, Durban, 4000, South Africa

[g] *P. Mente*
Institute for Catalysis and Energy Solutions, University of South Africa, Florida 1709, South Africa

Supporting information for this article is available on the WWW under https://doi.org/10.1002/slct.202303328

over, *Escherichia coli* (*E. coli*) has also developed resistance towards ampicillin, kanamycin, sulfisoxazole, streptomycin, tetracycline, and ticarcillin.[14] As a proof of concept, the antimicrobial effect of AgNPs with improved activity against both gram- (positive and negative) bacterial strains has been reported in various studies.[15–18] As a result, AgNPs have also been used in many other applications, including but not limited to wound healing.[19,20] AgNPs are incorporated in wound dressings or added in ointments in wound healing. This incorporation has been reported to help prevent bacterial infection and reduce pain.[21] However, the cytotoxicity of AgNPs towards healthy cells can be their limiting factor in various biomedical and related fields. Hence, controlling the concentration, sizes, and other parameters of AgNPs is crucial.

The cytotoxicity of AgNPs is yet to be addressed in full, with consistent results. Various studies have investigated the toxicity of AgNPs while varying parameters such as shapes, sizes and the concentration of the NPs.[22] It was found that AgNPs with diameters of 10 nm affected the cell viability of human lung cells compared to those of 40, 50, and 75 nm.[22] Another study reported reduced cell viability in human mesenchymal stem cells due to AgNPs with a concentration of 10 μg/mL and particle diameter of < 50 nm.[23] Contrary to the above reports, the non-toxic nature of AgNPs at a concentration of about 100 μg/mL with the particle size range of 10–20 nm was observed.[24] Although AgNPs possess several advantages that render them promising materials for various applications, they are less stable than other coinage metallic nanomaterials and tend to agglomerate with time. Agglomerated AgNPs are known to be more toxic against healthy cells compared to well-suspended AgNPs.[25] Therefore, the synthesis of stable AgNPs is of great importance and can yield more desirable results in their applications. To address the stability challenges posed by AgNPs, researchers have introduced various stabilizing/capping agents to minimize agglomeration.

Various methods for synthesizing stable AgNPs have been reported in the literature.[26,27] The use of organic compounds from plant extracts such as yerba mate; and polymers such as polyvinylpyrrolidone as capping and reducing agents in the synthesis of AgNPs have been found to play a significant role in stabilizing the NPs, hence resulting in no signs of agglomeration.[28–33] Dopamine (DA) is an organic compound that functions as hormones and neurotransmitters in the body and brain. DA is biocompatible, and it could be less toxic compared to other capping agents when used in the synthesis on NPs.[34–36] Moreover, the compound exhibits a notable abundance of catechol and N–H functional groups. These distinctive chemical moieties have demonstrated their efficacy in the reduction of metal ions, as affirmed not only by our preceding investigation but also by complementary studies conducted by various researchers.[37,38] This study, therefore, reports on the controlled synthesis of DA-capped AgNPs (AgNPs-DA) of various sizes and further investigates their antimicrobial activity and cytotoxicity. DA not only serves as a reducing agent but also plays a crucial role in stabilizing the synthesized AgNPs. The presence of DA on the surface of the AgNPs helps control their growth and prevents uncontrolled agglomeration. This is particularly important for achieving uniform particle size distribution, as well as for enhancing the reproducibility and scalability of the synthesis process. The antimicrobial activities of AgNPs-DA were investigated against *E. coli* and *S. aureus* bacterial strains. AgNPs-DA has shown excellent antimicrobial activity against both bacterial strains at relatively low concentrations. The cytotoxicity of the NPs towards human embryonic kidney (HEK-293T) cells was further investigated. It was noticed that AgNPs-DA did not have a significant toxic effect on the cells with a viability of over 70% at the concentration of 27 μg/mL. In addition, the Zeta potentials of NPs were determined, and their stability was explained following the DLVO theory

2. Methods

2.1. Materials

Silver nitrate ($AgNO_3$), dopamine hydrochloride, Luria Bertani Broth (LB), Tryptic Soy Agar (TSA), HEK-293T, Dulbecco's Modified Eagle Medium (DMEM) and fetal bovine serum (FBS) were all purchased from Sigma Aldrich and used as received. All glassware was washed with aqua-regia and rinsed with distilled water.

2.2. Preparation of AgNPs

AgNPs were synthesized using DA as a reducing agent and silver nitrate ($AgNO_3$) as Ag precursor. In a typical procedure, $AgNO_3$ solutions with various concentrations (0.05, 0.1, 0.5 and 1 mM) were prepared in 100 mL distilled water, separately. The solutions were then heated to boil, followed by adding 1 mL of dopamine hydrochloride (0.1 mM). The reactions were carried out for 5 min while stirring. The products were cooled and washed 2 times with distilled water using a centrifugation method before characterization. A stable pale-yellow colour confirmed the formation of colloidal AgNPs-DA.

2.3. Cell viability studies

The toxicity of AgNPs against mammalian cells was determined using the HEK-293T cell line, and cell viability was assessed using the MTS cell proliferation assays. HEK-293T cells were cultured in DMEM supplemented with 10% FBS and 1% penicillin-streptomycin antibiotic solution. The cells were grown in a 37 °C incubator with a humidified atmosphere of 5% CO_2.

For the assay, the cells were seeded at a density of $1x10^6$ cells/mL and a final volume of 100 μL/well in 96-well tissue culture plates. The cells were incubated at 37 °C under 5% CO_2 for 48 h to allow for stabilization. Two-fold serial dilutions of AgNPs-DA in complete culture media were introduced, with final concentrations on the plates ranging between 1.7–215 μg/mL. The plates were incubated under standard culture conditions for 48 h, after which the viability of

the cells was determined using the MTS dye. At a volume of 20 μL/well, the MTS solution was added, and the plates were incubated at 37 °C for an additional 4 h. The optical density (OD) was then determined at 490 nm using a plate reader, and untreated HEK-293T cells (cells without AgNPs-DA) were used as a positive control. To achieve statistical viability, all experiments were conducted in triplicate. The percentage of viable cells (%Viability) was calculated using the following equation:

$$\%\text{Viability} = \frac{Absorbance\ of\ Sample - Absorbance\ of\ Medium}{Absorbance\ of\ Control - Absorbance\ of\ Medium}\ X\ 100$$

2.4. Antimicrobial activity tests

2.4.1. Well diffusion method

The antimicrobial activity of the materials was tested using the conventional well-diffusion method against *E. coli* and *S. aureus*. The bacterial strains were inoculated to the LB Broth and cultured in a shaking incubator at 37 °C and 250 rpm overnight. The bacterial cultures were then spread-plated onto TSA plates. Wells were made on the plates using a cork borer, and 100 μL of AgNPs-DA (30 μg/mL) solution was added to the wells. After incubation at 37 °C for 18–24 h, the zones of inhibition were measured using a ruler.

2.4.2. Minimum inhibitory concentration (MIC) and bacteriostatic studies

The standard broth dilution method was used to determine the MIC of the as-synthesized AgNPs-DA. Two-fold dilutions of AgNPs-DA (0.49, 0.94, 1.875, 3.75, 7.5, 15 and 30 μg/mL) were prepared in a broth solution dispensed inside sterilized test tubes containing minimum volume of 2 mL. Each tube was inoculated with the bacteria (*E. coli or S. aureus*). The concentration of bacterial was adjusted to $1x10^6$ CFU/mL using the McFarland method. After gentle mixing, the tubes were incubated at 37 °C for 24 h while shaking at 250 rpm. The MIC is the lowest concentration of AgNPs-DA that completely inhibits bacterial growth in the tubes which was detected by an eye.

To determine the bacteriostatic effect, the MIC of AgNPs-DA was prepared in a broth solution dispensed inside sterilized test tubes followed by inoculation with bacterial strains. The OD of the inoculated broth containing AgNPs-DA was measured at the absorbance of 600 nm and used as reference. Therefore, the tubes were incubated at 37 °C for 24 h while shaking at 250 rpm and the day 1 OD was measured. The study was conducted over 14 days and in triplicate.

2.5. Characterization techniques

All excess impurities from colloidal solutions were removed using a universal 320R centrifuge at a maximum speed of 15000 rpm. The Chemical structure analysis of the material was conducted using a Bruker Tensor 27 Fourier transform infrared (FTIR) spectrometer. The absorption spectra were acquired using a Varian Cary Eclipse (Cary 50) UV-vis spectrophotometer. Transmission electron microscopy (TEM) images were obtained from FEI Tecnai-T12 microscopy at an electron acceleration voltage of 120 kV and beam spot size of 10–100 nm and the sizes of the NPs were determined using ImageJ software. More than 100 NPs (for the different samples) were measured from the TEM images. PXRD analysis was performed on a Bruker D2 Phaser with Cu Kα radiation source. Each scan was recorded for 20 min. The Zeta potentials of the NPs were obtained from a Malvern Zetasizer nano series using folded capillary cell (DTS1070).

3. Results and discussion

3.1. AgNPs-DA characterization

DA was used as the reducing and capping agent in this study. The oxidation of the catechol groups in DA was responsible for reducing silver (Ag) ions. During the oxidation process, the two catechol groups lose electrons, which end up reducing the Ag ions and the resulting quinone compounds adsorb on the surface of AgNPs-DA. To study the chemical structure of the synthesized AgNPs-DA, chemical analysis was conducted using FTIR. Figure 1 shows the FTIR spectra of DA and AgNPs-DA of various sizes. The DA spectrum exhibited well-defined characteristic functional groups represented by well pronounced peaks at high and lower wavenumbers. The broad bands at approximately 3341 cm^{-1}, 3165 cm^{-1} and 3089 cm^{-1} were attributed to amine N–H, phenolic O–H and aromatic C–H stretching modes, respectively. The band at 2950 cm^{-1} was due alkyl C–H stretching. The bands observed at 1605 cm^{-1}, 1498 cm^{-1} and 1265 cm^{-1} were attributed to amine N–H bending, aromatic C=C stretching and phenolic C–O stretching. The AgNPs-DA FTIR spectra show similar bands which are shifted towards higher energies. The shift in the vibrational bands could be due to the interaction of the O groups with the surface of AgNPs. More bands were observed in the spectra of AgNPs-DA. The band at 2151 cm^{-1} could be due to the possible formation of allene-like structure resulting from the electron delocalization in the DA-o-semiquinone intermediates. The vibrational band around 1997 cm^{-1} was assigned to the bending modes of aromatic C–H groups. The peak around 2348 could be due to the atmospheric CO_2. CO_2 is one of the gases that are IR active.

Figure 2 shows the TEM micrographs of AgNPs-DA. The as-synthesized AgNPs-DA were spherical-like in shape, with average diameters of 16 nm, 24 nm, 48 nm and 74 nm, as shown in Figure 2 (A, B, C and D), respectively. Figure S1 shows the particle size distribution of the AgNPs-DA. The wide range

Research Article
doi.org/10.1002/slct.202303328
Chemistry Europe
European Chemical Societies Publishing

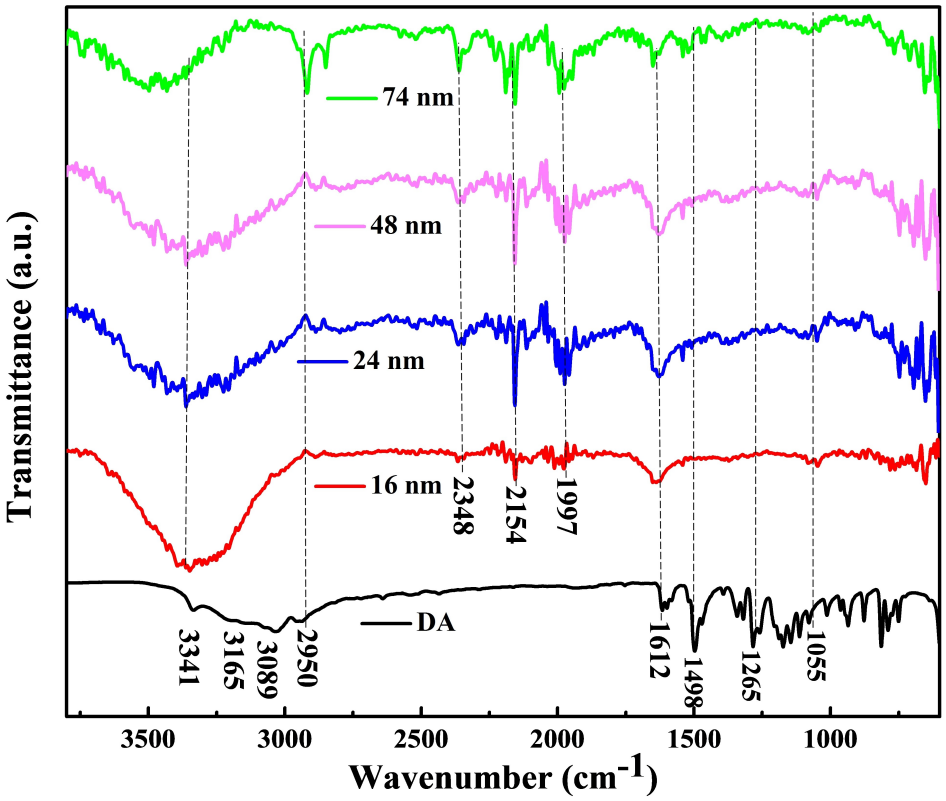

Figure 1. FTIR spectra of DA and the synthesized AgNPs-DA.

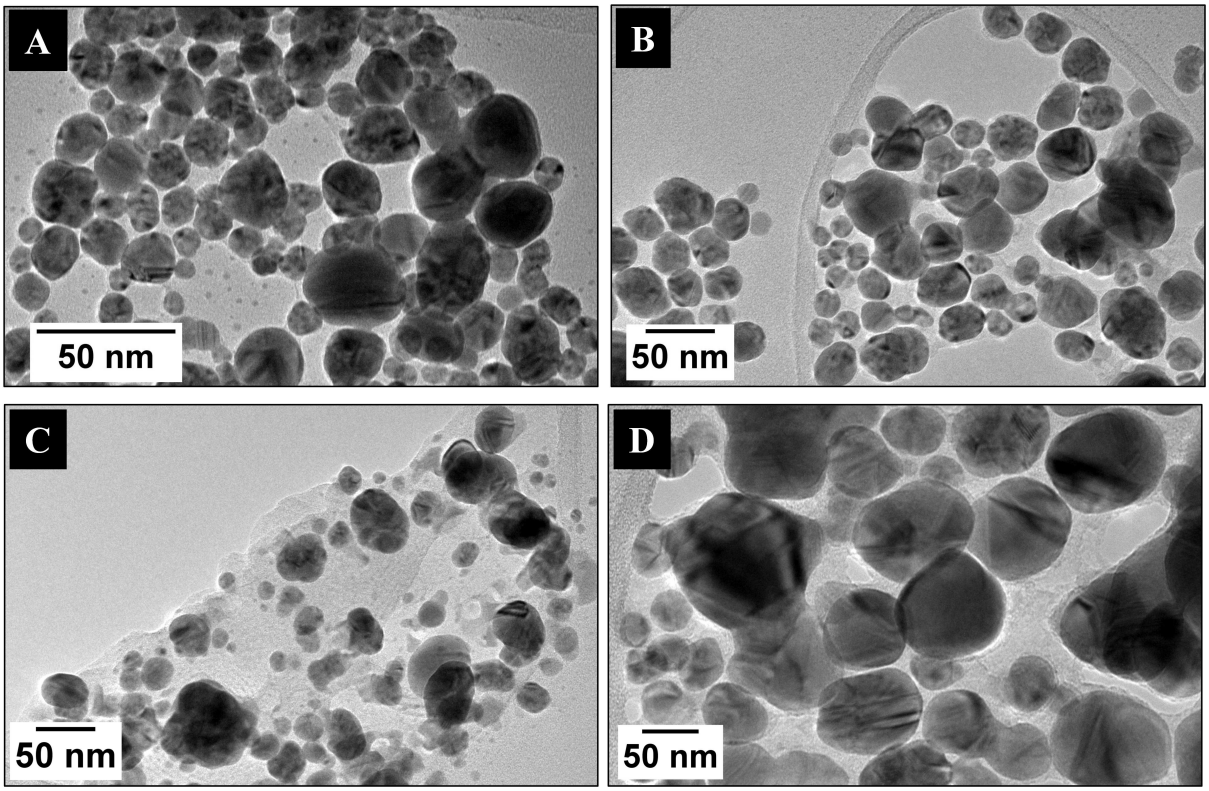

Figure 2. TEM images (A = 16 nm, B = 24 nm, C = 48 nm, D = 74 nm) of DA capped AgNPs synthesized at different $AgNO_3$ concentrations.

of NPs diameters with relatively high standard deviations observed from their size distribution signify polydispersity of the NPs. The sizes of the NPs increased with an increase in the concentration of $AgNO_3$. At a high concentration of $AgNO_3$, more Ag ions get reduced and nucleated, resulting in the fast growth of AgNPs through Ostwald ripening.[39]

UV-vis absorption spectrometry was used to study the optical properties of the synthesized AgNPs-DA. The UV-vis absorption spectra of AgNPs-DA synthesized at different $AgNO_3$ concentrations are shown in Figure 3. The characteristic surface plasmon resonance (SPR) bands were observed with maxima peaks appearing at 416, 432, 418 and 435 nm for AgNPs-DA with an average diameter of 16, 24, 48 and 74 nm, respectively. The presence of the SPR bands indicates the successful formation of AgNPs-DA. A clear and significant shift to higher wavelengths (Red shift) was observed as the size of AgNPs increased. The red shift of the absorption bands was attributed to the increase in the particles diameter. Larger nanoparticles exhibit a long range of energy level for electronic transitions. Therefore they absorb energy ant lower energy or towards longer wavelength.

The zeta potentials of the NPs were determined using a Zetasizer to evaluate their surface charge and ionic strength. The ionic strength can be used to determine their stability. Generally, the colloidal NPs with zeta potential above +60 mV and below −60 mV are considered highly stable, while those above +20 mV and below −20 mV are reasonably stable.[28] As shown in Figure S2, zeta potentials of AgNPs-DA were −20.3, −23.4, −25.6 and −26.5 mV for AgNPs-DA with the average diameters of 16, 24, 48 and 74 nm, respectively. These findings indicate that the NPs are reasonably stable. The negative zeta potentials suggest that the surface of the AgNPs-DA is negatively charged. This can be attributed to the adsorption of dopamine-semi-o-quinone anions on the surface of NPs because of DA oxidation. It is important to note that the zeta potential of the NPs increased with their diameter. This means that NPs with a small diameter (16 nm) are less stable than bigger particles. This data is per the DLVO theory, which determines the total potential energy by summing the contributions from the van der Waals attraction and the electric double layer repulsion. According to the DLVO predictions, the smaller particles are more prone to agglomeration due to the decrease of interaction potential with particle size.[40] The other explanation for the low stability of AgNPs-DA with an average diameter of 16 nm can be the high surface energy posed by smaller NPs in colloids. Due to the high surface energy of small NPs, the activation energy gets lowered due to decreasing surface charge, leading to particles agglomeration.[41] In addition, the inherent stability of small NPs gets compromised due to their high specific surface area and a large fraction of surface atoms which promotes more reactive sites.[42]

PXRD was used to investigate the crystallinity and structural phase of AgNPs-DA. The diffraction patterns of AgNPs-DA are shown in Figure 4. The diffraction patterns show diffraction peaks at 38.09°, 44.35°, 64.48°, 77.39° and 81.72° 2θ values, corresponding to (111), (200), (220), (311) and (222) lattice planes of face centred cubic (FCC) crystal structure of metallic Ag, respectively. The presence of the above peaks confirms the successful synthesis of AgNPs. However, as the concentration of $AgNO_3$ increased, some peaks that were not due to metallic Ag (denoted by *) were observed. The presence of those unassigned peaks resulted from silver chloride (AgCl). When

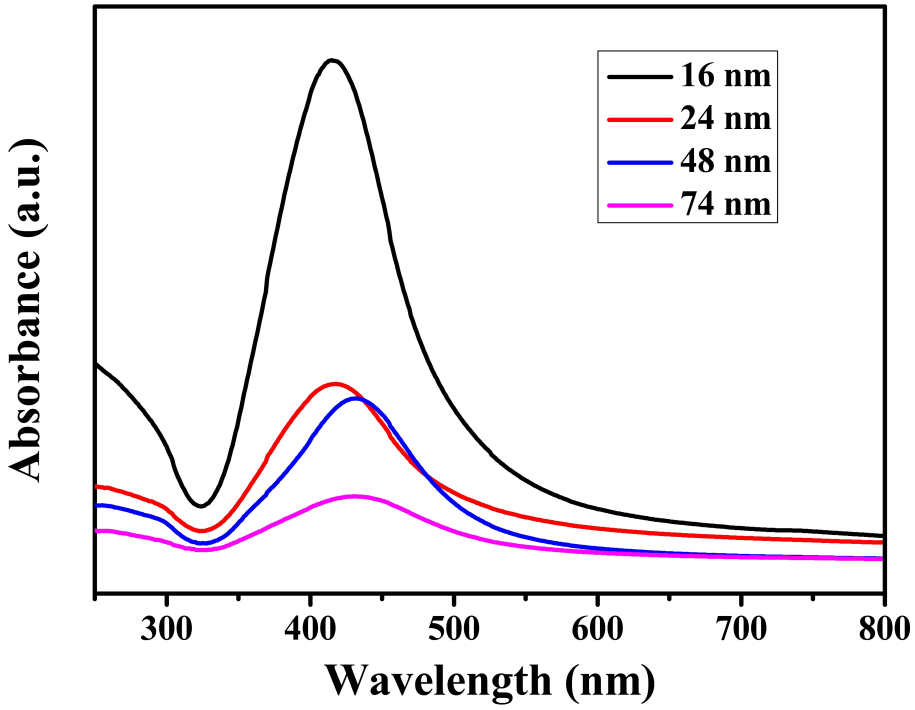

Figure 3. UV-vis absorption spectra of AgNPs-DA of various sizes.

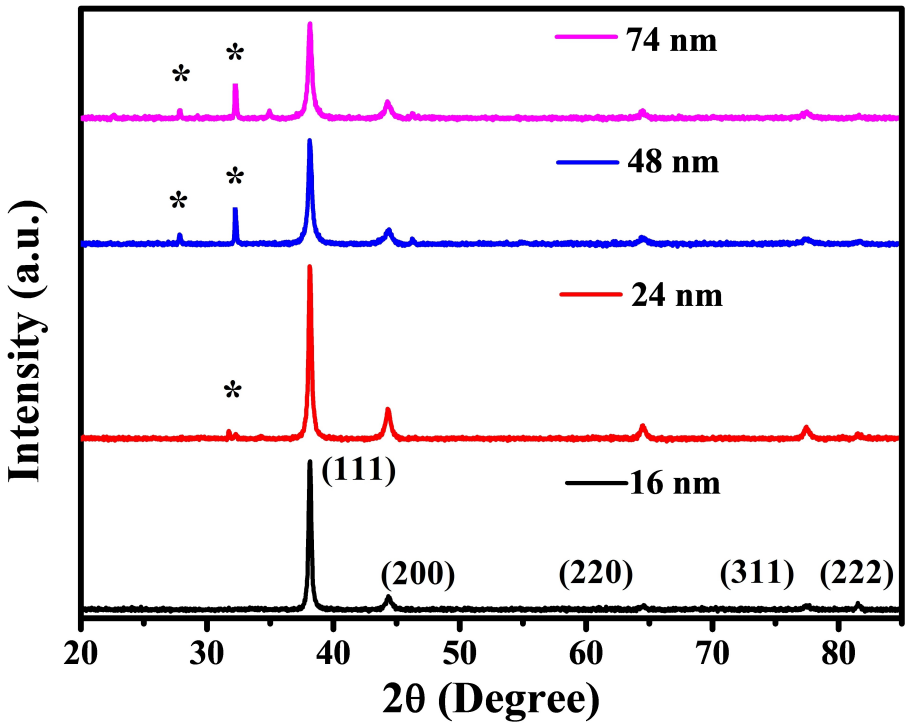

Figure 4. The PXRD patterns of AgNPs-DA showing Ag (PDF: 01–071-4612) and AgCl (* PDF: 00–031-1238) with the average diameters of 16 nm, 24 nm, 48 nm and 74 nm.

dopamine hydrochloride oxidizes, most Ag ions get reduced into their zerovalent state. The excess Ag ions interact with the chlorine ions to form crystalline AgCl.

3.2. Toxicity studies of AgNPs-DP

The MTS assay was used to evaluate the toxicity of AgNPs-DA. This was done by assessing the viability of HEK-293T cells following treatment with AgNPs-DA at various concentrations for a period of 72 h. The concentration of AgNPs-DA played a significant role in their toxicity compared to their sizes. This is illustrated in Figure 5, which shows the viability of HEK-293T cells plotted against the concentration of AgNPs-DA with different sizes. A decrease in cell viability was observed as the concentration of AgNPs-DA was increased. Initially, the HEK-293T cells showed good viability at a concentration range of 2 to 27 μg/mL. At this range, the cell viabilities were over 60%. A drastic decrease (below 40%) of cell viability was observed when the concentration of AgNPs-DA was increased to 54 μg/mL. A further decrease (below 30%) was observed as the concentration increased to 108 μg/mL, which signifies that the as-synthesized AgNPs-DA become toxic when the concentration exceeds 50 μg/mL, regardless of the size. Similar findings were previously reported. In their study, AgNPs showed the concentration-dependent cell viability in renal epithelial (A498) and hepatic (Hep G2) cell lines.[43] No clear trend was observed concerning the effect of AgNPs-DA sizes as the cell viability fluctuates. However, a slight trend was observed at high concentrations of AgNPs-DA. Cell viability decreased with a decrease in the size of AgNPs-DA at the concentration of 54 and 108 μg/mL. In a separate study, it was also observed that AgNPs with small sizes pose a more negative impact on cell viability than bigger particles,[44] which is in concise agreement with our observations, even though the trend was only apparent at high concentrations.

Figure 6 represents the sigmoid curves of HEK-293T cells treated with 16 nm, 24 nm, 48 nm and 74 nm AgNPs-DA. These were used to determine the 50% cytotoxic concentration (CC_{50}) values of AgNPs-DA. The CC_{50} value is defined as the concentration of AgNPs-DA that has reduced the cell viability by 50%. As shown in Table 1, the CC_{50} values for 16, 24, 48 and 74 nm AgNPs-DA were 22.4, 30.9, 18.9 and 21.4 μg/mL, respectively. The CC_{50} values obtained show that AgNPs-DA did not significantly affect the HEK-239T cells. There was no clear trend observed between CC_{50} values and the sizes of NPs, as was the case with the cell viability in Figure 5.

3.3. Antimicrobial activity of AgNPs-DA

The antimicrobial activity of AgNPs-DA was determined by a standard well-diffusion method against *E. coli* and *S. aureus* bacteria. Figure 7 shows the photographed images of the agar plates with clear zones of inhibition around the wells. The effect of AgNPs size on the inhibition of bacterial growth was observed. Table 1 summarizes the zones of inhibition measured using ImageJ software, which range from 9 mm to 17 mm in diameter. The size-dependent antimicrobial activity of the as-synthesized AgNPs-DA against *E. coli* and *S. aureus* was

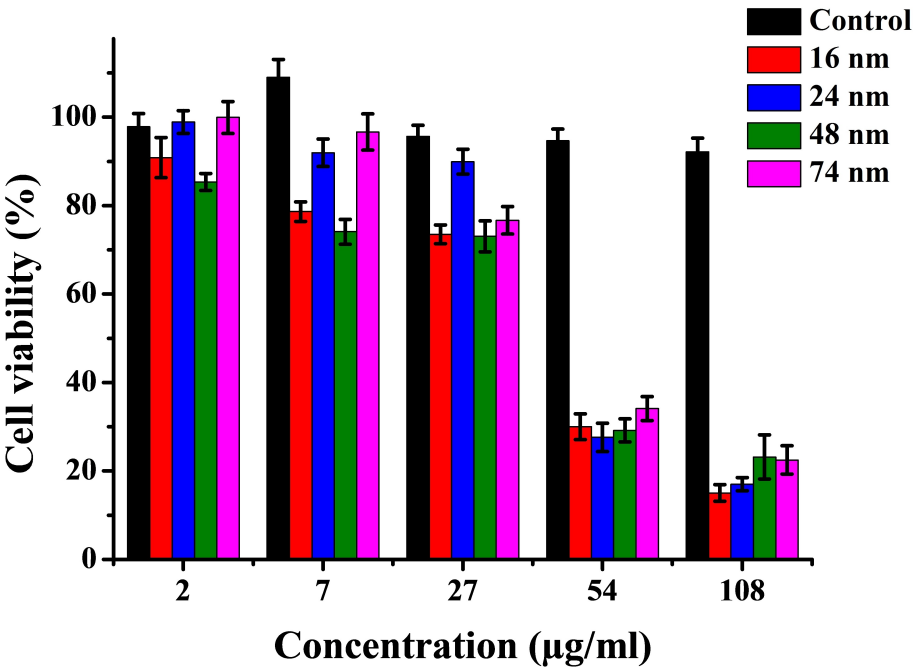

Figure 5. Cell viability of HEK-293T cells exposed to AgNPs-DA of different sizes at different concentrations.

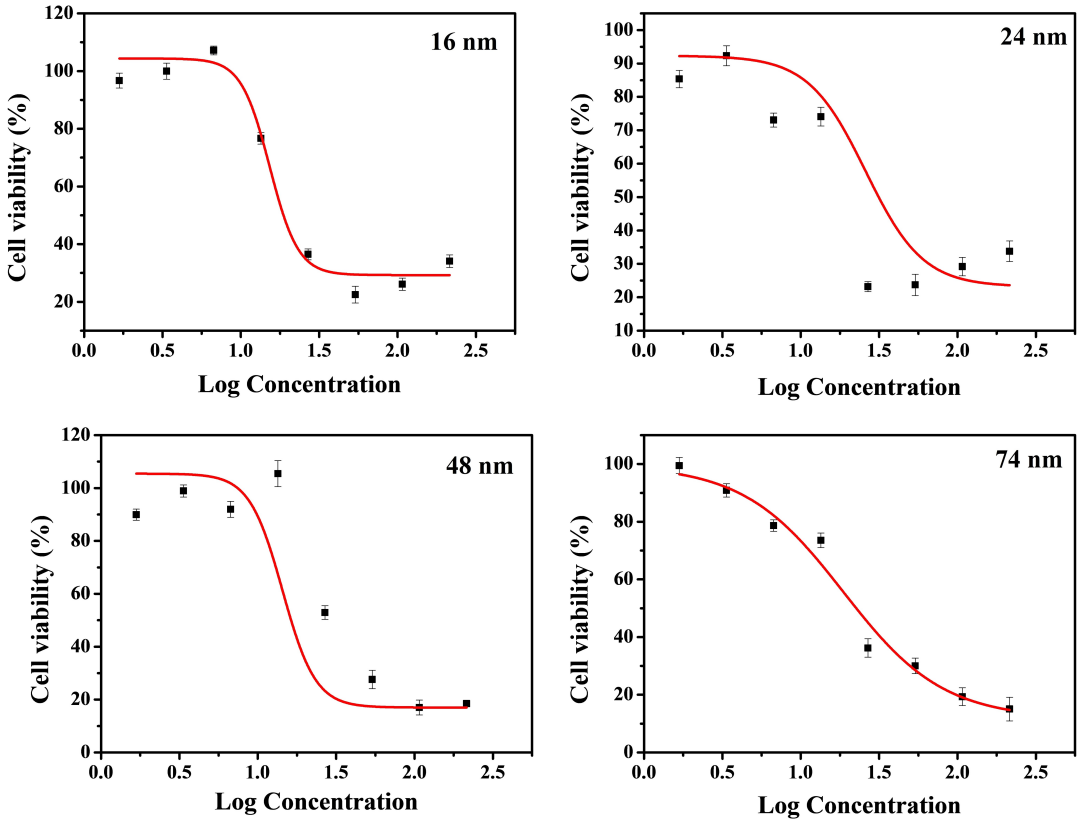

Figure 6. The sigmoid curves of cell viability acquired by incubating HEK-293T cells with 16 nm, 24 nm, 48 nm and 74 nm AgNPs-DA at different concentrations.

observed. The sizes of the zones of inhibition were observed to increase as AgNPs-DA average diameters decreased, indicating that smaller sized AgNPs-DA are more potent compared to bigger ones. This is attributed to the fact that NPs with smaller sizes have a high surface area to volume ratio, making it easier for them to penetrate the bacterial cell wall and interact with

Table 1. Summary of the inhibition zones, MIC and CC_{50} of the AgNPs-DA of various sizes.

Sample	Zone of Inhibition (mm)		MIC (μg/mL)		CC_{50} (μg/mL)
	E. coli	*S. aureus*	*E. coli*	*S. aureus*	
16 nm	17	15	3.75	3.75	22.4
24 nm	14	13	7.5	7.5	30.9
48 nm	12	10	15	15	18.9
74 nm	10	9	15	15	21.4

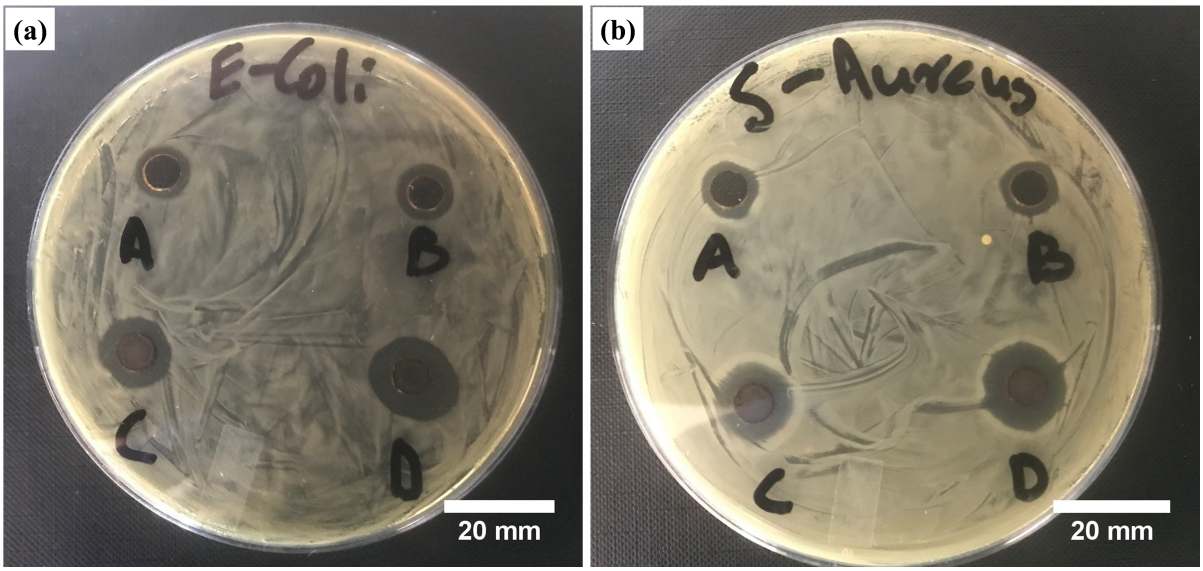

Figure 7. Visible inhibitory Zones produced by (A) 74 nm, (B) 48 nm, (C) 24 nm and (D) 16 nm AgNPs-DA against (a) E. coli and (b) S. aureus. Scale bar = 20 mm.

vital organelles within the cell. Furthermore, the surface energy of the smaller particles makes them more reactive. This can results in small particles reacting with vital organelles such sulphur containing proteins and nucleic acids as reported earlier on.[37] In addition, the ability of AgNPs to release Ag ions (Ag^+) when in contact with the bacteria plays a vital role in their toxic effect on bacteria cells. The release of Ag^+ ions also facilitates the interaction of Ag with vital cell organelles, which are lethal to bacteria. The comparison of the antimicrobial activity of the zerovalent Ag (Ag^o) and Ag^+ has been conducted in literature.[45–47] Table 2 shows more studies that have reported on the antimicrobial activity of capped AgNPs with some comparison with the current AgNPs-DA. The inhibitory effect of the NPs was stronger against *E. coli* than *S. aureus*, as indicated by the more extensive zones of inhibition in *E. coli* compared to *S. aureus*. This may be due to the different cell membranes of the gram-positive and gram-negative bacterium. Gram-negative bacteria have a thinner peptidoglycan layer than gram-positive

Table 2. Comparison of antimicrobial performance of AgNPs-DA with related literature.

Material	Antimicrobial performance			References
	ZOI (mm)	MIC μg/mL	Bactericidal or bacteriostatic	
AgNPs-DA	17	3.75	Bacteriostatic (Over 14 days)	Current study
AgNPs-Starch	–	1.39	Not specified	48
AgNPs-chitosan/algae	10–21	-	Not specified	49
AgNPs-Chitosan/pectin	18.2	-	Not specified	50
AgNP/PVA/BNC	–	-	Bacteriostatic (Over 1 days)	51
AgNPs-DA-gelatine-PEG	16.5	-	Not specified	52
AgNPs-Polydopamine	15.1	-	Not specified	53

bacteria, making it easier for NPs to penetrate gram-negative bacterial strains.

The serial dilution method determined the minimum inhibitory concentrations (MIC) of AgNPs-DA of different sizes. In the 8 test tubes filled with LB broth, AgNPs-DA and either *E. coli* or *S. aureus* bacterial strain, four of them appeared cloudy or turbid, while the remaining four appeared clear. The cloudy appearance in the test tubes indicates bacterial growth, whereas the clear appearance shows the inhibition of bacterial growth by AgNPs-DA. Therefore, the MIC values of AgNPs-DA were obtained from the fourth clear tube. The MIC values are summarized in Table 1. AgNPs-DA with smaller sizes exhibited the lowest MIC values, indicating that small-sized NPs inhibit bacterial growth at lower concentrations compared to bigger sized-NPs. The optical density (OD) of bacterial strains treated with AgNPs-DA of different concentrations was monitored, as shown in Figure 8. The OD of untreated bacterial strains was acquired to make a fair comparison. In this case, the OD represents the concentration of bacteria. The OD of untreated bacterial strains was as high as 2 a.u, which shows the high concentration of bacteria. The OD of bacterial strains treated with AgNPs-DA decreases gradually to almost zero. The OD remained almost zero as the concentration of AgNPs-DA increased. The slight increase in OD at higher concentrations can be attributed to the absorbance of AgNPs-DA. These observations were made in all AgNPs-DA sizes. It can be observed from Figure 8 that the MICs of AgNPs-DA with small sizes is lower compared to those of larger sized NPs. These results highlight the high efficacy of smaller sized NPs compared to those of bigger sizes.

The bacteriostatic effects of AgNPs-DA were further evaluated. To conduct this study, bacterial solutions (in LB broth) were treated with NPs and allowed to incubate for 14 days, with sampling every 24 h to investigate the OD of the solutions. An increase in OD of the bacterial solution indicates an increase in the number of bacteria. Figure 9 shows the bar graphs representing the bacteriostatic effects of the AgNPs-DA. The bar graphs A, B, C and D represent the bacteriostatic effects of 74 nm, 48 nm, 24 nm and 16 nm AgNPs-DA against (a) *E. coli* and (b) *S. aureus*. The bacterial growth was very low on day 1, indicating the prevention of bacterial growth by AgNPs-DA of various sizes. The OD gradually increased on day 2, with further or continuous increase as days went by for 74 nm and 48 nm AgNPs-DA. This indicates that AgNPs-DA with larger sizes lost their antibacterial activity within the first 24. The increase in OD is another way of showing the bacterial growth in the samples.

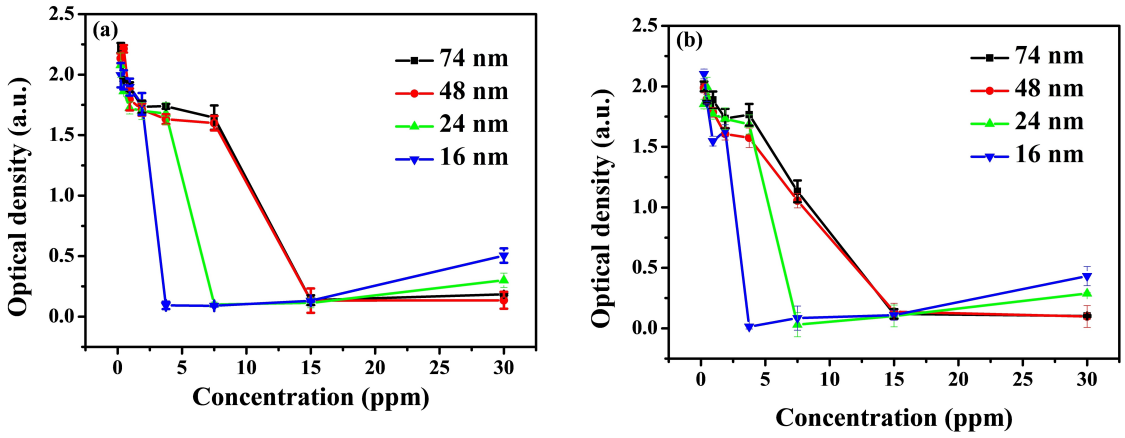

Figure 8. The relationship between bacterial growth (OD) and the concentration of AgNPs-DA of different sizes, tested against (a) *E. coli* and (b) *S. aureus*.

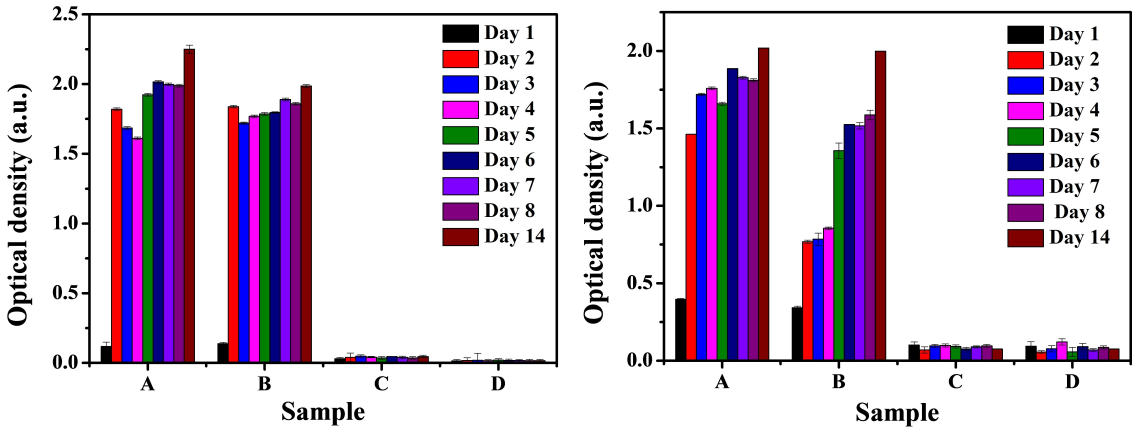

Figure 9. The bar graph representation of the bacteriostatic effect of (A) 74 nm, (B) 48 nm, (C) 24 nm and (D) 16 nm AgNPs-DA against (a) *E. coli* and (b) *S. aureus*.

AgNPs-DA with smaller sizes (16 nm and 24 nm) showed an excellent bacteriostatic ability for *E. coli* and *S. aureus*. Even after 14 days, there was no indication of bacterial growth. This signifies that smaller NPs could strongly suppress bacterial growth than bigger NPs. It is important to note that the ODs were smaller on the *E. coli* than the *S. aureus* for the 16 nm and 24 nm AgNPs-DA, further illustrating higher sensitivity of *E. coli*, as explained earlier. Due to their ability to inhibit bacterial growth, AgNPs-DA can be applied in various applications such as wound healing or water purification.

4. Conclusions

This study successfully highlighted the straightforward size-controlled synthesis of AgNPs using DA as both the reducing and capping agent. The obtained AgNPs-DA were spherical-like in shape, as evident from TEM analysis. The optical studies confirmed the successful synthesis of AgNPs-DA as denoted by the SPR bands in the UV-vis spectra. The PXRD analysis showed that AgNPs with FCC structural phase were obtained. The cytotoxicity of the as-synthesized AgNPs-DA against HEK-293T cells was investigated. AgNPs-DA of different sizes showed concentration-dependent cytotoxicity. The cell viability of the HEK-293T cells was highly compromised by AgNPs-DA of all the sizes/diameters at concentrations above 54 μg/mL. The CC_{50} values of AgNPs-DA were relatively high, which indicates the low toxic nature of AgNPs-DA against the HEK-293T cells. The synthesized AgNPs-DA were found to pose an interesting antimicrobial activity against *E. coli* and *S. aureus*. AgNPs-DA with smaller sizes were more effective in inhibiting bacterial growth than the bigger ones, as evident from their bacterial inhibition zones. In addition, smaller AgNPs-DA were found to have low MIC values compared to the bigger NPs. Most interestingly, these AgNPs-DA can keep both *E. coli* and *S. aureus* dormant for over 14 days. Bioactive materials like AgNPs-DA can be suitably and safely applied in wound healing applications to prevent bacterial infection, or even as one of the active ingredients in the antibiotics (at monitored concentrations) to improve their life span and activity.

Acknowledgements

The authors would like to acknowledge the University of the Witwatersrand, School of Chemistry, for conducting research work in the School's laboratories. We would also like to thank the DSI/Mintek Nanotechnology Innovation Centre and the Centre for Metal-based Drug Discovery for allowing us to use their facilities for antibacterial and cytotoxicity studies, respectively. This work was financially supported by the National Research Foundation (NRF) of South Africa.

Conflict of Interests

I declare that all authors have no interest in conflict regarding the publication of this work.

Data Availability Statement

The data that support the findings of this study are available from the corresponding author upon reasonable request.

Keywords: Silver · Dopamine · Zeta potential · Stability · Bacteriostatic

[1] M. A. Dar, A. Ingle, M. Rai, *Nanomed-Nanotechnol.* **2013**, *9*, 105–110.
[2] J. Huang, Q. Li, D. Sun, Y. Lu, Y. Su, X. Yang, H. Wang, Y. Wang, W. Shao, N. He, J. Hong, C. Chen, J. Huang, *Nanotechnology.* **2017**, *18*, 105104.
[3] A. M. Díez-Pascual, *Nanomaterials.* **2020**, *10*, 2315.
[4] K. Yang, Q. Han, B. Chen, Y. Zheng, K. Zhang, Q. Li, J. Wang, *Int. J. Nanomed.* **2018**, *13*, 2217–2263.
[5] R. Banasiuk, J. E. Frackowiak, M. Krychowiak, M. Matuszewska, A. Kawiak, M. Ziabka, Z. Lendzion-Bielun, M. Narajczyk, A. Krolicka, *Int. J. Nanomed.* **2016**, *11*, 315–324.
[6] P. Dube, S. Meyer, A. Madiehe, M. Meyer, *Nanotechnology.* **2020**, *31*, 505607.
[7] M. O. Ilomuanya, A. Adebona, W. Wang, A. Sowemimo, C. L. Eziegbo, B. O. Silva, S. O. Adeosun, E. Joubert, D. De Beer, *SN Appl. Sci.* **2020**, *2*, 1–13.
[8] T. Cheng, S. Lin, L. Chen, H. Chen, *Food Packag. Shelf Life.* **2018**, *16*, 129–137.
[9] M. J. Hortigüela, L. Yuste, F. Rojo, I. Aranaz, *Nanomaterials.* **2016**, *6*, 137.
[10] M. V. D. Z. Park, A. M. Neigh, J. P. Vermeulen, L. J. J. de la Fonteyne, H. W. Verharen, J. J. Briedé, H. Loveren, W. H. de Jong, *Biomaterials* **2011**, *32*, 9810–9817.
[11] K. N. J. Stevens, O. Crespo-Biel, E. E. M. van den Bosch, A. A. Dias, M. L. W. Knetsch, Y. B. J. Aldenhoff, F. H. van der Veen, J. G. Maessen, E. E. Stobberingh, L. H. Koole, *Biomaterials.* **2009**, *30*, 3682–3690.
[12] N. A. Feasey, K. Gaskell, V. Wong, C. Msefula, G. Selemani, S. Kumwenda, T. J. Allain, J. Mallewa, N. Kennedy, A. Bennett, J. O. Nyirongo, *PLoS Neglected Trop. Dis.* **2015**, *9*, p.e0003748.
[13] M. Schaller, J. Laude, H. Bodewaldt, G. Hamm, *Skin Pharmacol. Physiol.* **2004**, *17*, 31–36.
[14] J. Meng, S. Zhao, M. P. Doyle, S. W. Joseph, *J. Food Prot.* **1998**, *61*, 1511–1514.
[15] K. Vimala, Y. M. Mohan, K. Varaprasad, N. N. Redd, S. Ravindra, N. S. Naidu, K. M. Raju, *J. Biomater. Nanobiotechnol.* **2011**, *2*, 55–64.
[16] S. Rajeshkumar, C. Malarkodi, M. Vanaja, G. Annadurai, *J. Mol. Struct.* **2016** *1116*, 165–173.
[17] S. Islam, B. S. Butolab, F. Moh, *RSC Adv.* **2016**, *6*, 44232–44247.
[18] L. Liu, J. Yang, J. Xie, Z. Luo, J. Jiang, Y. Y. Yang, S. Liu, *Nanoscale.* **2013**, *5*, 3834–3840.
[19] K. Kalantari, E. Mostafavi, A. M. Afifi, Z. Izadiyan, H. Jahangirian, R. Rafiee-Moghaddam, T. J. Webster, *Nanoscale.* **2020**, *12*, 2268–2291.
[20] K. H. L. Kwan, X. Liu, M. K. T. To, K. W. K. Yeung, C. Ho, K. K. Y. Wong, *Nanomed-Nanotechnol.* **2011**, *7*, 497–504.
[21] A. Gupta, S. M. Briffa, S. Swingler, H. Gibson, V. Kannappan, G. Adamus, M. Kowalczuk, C. Martin, I. Radecka, *Biomacromolecules.* **2020**, *21*, 1802–1811.
[22] A. R. Gliga, S. Skoglund, I. O. Wallinder, B. F. Karlsson, H. L. Karlsson, *Part. Fibre Toxicol.* **2014**, *11*, 1743–8977.
[23] S. Hackenberg, A. Scherzed, M. Kessler, S. Hummel, A. Technau, K. Froelich, C. Ginzkey, C. Koehler, R. Hagen, N. Kleinsasser, *Toxicol. Lett.* **2011**, *201*, 27–33.
[24] M. E. Samberg, E. G. Loboa, S. J. Oldenburg, N. A. Monteiro-Riviere, *Nanomedicine* **2012**, *7*, 1197–209.
[25] S. Kittler, C. Greulich, J. Diendorf, M. Koller, M. Epple, *Chem. Mater.* **2010**, *22*, 4548–4554.
[26] I. Pinzaru, D. Coricovac, C. Dehelean, E. Moacă, M. Mioc, F. Baderca, I. Sizemore, S. Brittle, D. Marti, C. D. Calina, A. M. Tsatsakis and C. Şoica, *Food Chem. Toxicol.* **2018**, *111*, 546–556.

[27] S. Khorram, A. Zarrab, M. Khaleghi, M. Danaei, M. R. Mozafari, *Int. J. Nanomed.* **2018**, *13*, 8013–8024.
[28] R. A. Arreche, G. M. de Oca-Vásquez, J. R. Vega-Baudrit, P. G. Vázquez, *Waste Biomass Valorization* **2018**, *11*, 245–253.
[29] A. G. Femi-Adepoju, A. O. Dada, K. O. Otun, A. O. Adepoju, O. P. Fatoba, *Heliyon* **2019**, *5*, e01543.
[30] R. Yan-yu, Y. Hui, W. Tao, W. Chuang, *Phys. Lett. A.* **2016**, *380*, 3773–3777.
[31] A. E. Mohammed, A. Al-Qahtani, A. Al-Mutairi, B. Al-Shamri, K. Aabed, *Nanomaterials.* **2018**, *8*, 382.
[32] S. V. Kumar, A. P. Bafana, P. Pawar, A. Rahman, S. A. Dahoumane, C. S. Jeffryes, *Sci. Rep.* **2018**, *8*, 1–10.
[33] S. B. Dalir, H. Djahaniani, F. Nabati, M. Hekmati, *Heliyon* **2020**, *6*, e03624.
[34] M. Sureshkumar, D. Y. Siswanto, Y. C. Chen, C. K. Lee, M. J. Wang, *J. Polym. Sci. Part B* **2013**, *51*, 303–310.
[35] S. Wang, W. Lu, O. Tovmachenko, U. S. Rai, H. Yu, P. C. Ray, *Chem. Phys. Lett.* **2008**, *463*, 145–149.
[36] P. C. Ray, H. Yu, P. P. Fu, *J. Environ. Sci. Health Part C* **2009**, *27*, 1–35.
[37] N. P. Shumbula, Z. B. Ndala, S. S. Nkabinde, S. Mpelane, P. M. Shumbula, P. S. Mdluli, Z. Njengele-Tetyana, P. Tetyana, T. Hlatshwayo, M. Mlambo, N. Moloto, *Arab. J. Chem.* **2022**, *15*, p.103798.
[38] H. Luo, C. Gu, W. Zheng, F. Dai, X. Wang, Z. Zheng, *RSC Adv.* **2015**, *5*, 13470–13477.
[39] D. K. Bhui, H. Bar, P. Sarkar, G. P. Sahoo, S. P. De, A. Misra, *J. Mol. Liq.* **2009**, *145*, 33–37.
[40] T. Y. He, J. Wan, T. Tokunaga, *J. Nanopart. Res.* **2008**, *10*, 321–332.
[41] A. S. Madden, M. F. Hochella JR, *Geochim. Cosmochim. Acta* **2005**, *69*, 389–398.
[42] K. Fukushi, T. Sato, *Environ. Sci. Technol.* **2005**, *39*, 1250–1256.
[43] H. Zhang, J. A. Smith, V. Oyanedel-Craver, *Water Res.* **2012**, *46*, 691–699.
[44] R. P. Singh, P. Ramarao, *Toxicol. Lett.* **2012**, *213*, 249–259.
[45] Z. M. Xiu, Z. M, J. Ma and P. J. Alvarez, *Environ. Sci. Technol.* **2011**, *45*, 9003–9008.
[46] O, Lyutakov, I. Goncharova, S. Rimpelova, Kolarova, J. Svanda and V. Svorcik, *Mater. Sci. Eng. C.* **2015**, *49*, 534–540.
[47] N. Durán, M. Durán, M. D. De Jesus, A. B. Seabra, W. J. Fávaro, G. Nakazato, *Nanomedicine Nanotechnology, Biol. Med.* **2016**, *12*, 789–799.
[48] V. Raji, M. Chakraborty, P. A. Parikh, *Part. Sci. Technol.* **2012**, *30*, 565–577.
[49] N. H. Rezazadeh, F. Buazar, S. Matroodi, *Sci. Rep.* **2020**, *10*, 19615.
[50] G. O. Akalin, O. Taner, T. Taner, *Polym. Bull.* **2021**, *79*, 1–18.
[51] W. Wang, Z. Yu, F. K. Alsammarraie, F. Kong, M. Lin, A. Mustapha, *Food Hydrocolloids* **2020**, *100*, 105411.
[52] T. N. Pham, Y. S. Jiang, C. F. Su, J. S. Jan, *Int. J. Biol. Macromol.* **2020**, *146*, 1050–1059.
[53] Z. Lu, J. Xiao, Y. Wang, M. MengJ Colloid, *Interface Sci.* **2015**, *452*, 8–14.

Manuscript received: August 22, 2023